Anion photoelectron spectroscopy of deprotonated indole and indoline

Daniel J. Nelson,[a] Allan M. Oliveira, and W. Carl Lineberger[b]
JILA and The Department of Chemistry and Biochemistry, University of Colorado Boulder, 440 UCB, Boulder, Colorado 80309, USA

(Received 9 September 2017; accepted 29 January 2018; published online 14 February 2018)

Anion photoelectron spectra of deprotonated indole have been obtained utilizing several photon energies. The slow electron velocity-map imaging spectrum of indolide allows for the determination of the electron affinity (EA) of indolyl, 2.4315 ± 0.0017 eV. The equilibrium geometry of indolide was shown to minimally distort upon photodetachment with only ring distortion vibrational modes of A' symmetry becoming significantly excited. Photoelectron spectra of indolide accessing the electronic ground state of indolyl displayed a photon energy dependence due to electron autodetachment. Combining the EA of indolyl with the previous work studying the dissociation energy of H-indolyl allows for a new independent measure of $\Delta_{acid}H^{o}_{0K}(N–H)_{indole} \leq 348.7$ kcal/mol, which improves the previous measurement of the gas phase acidity. The anion photoelectron spectrum of deprotonated indoline consisted of a featureless broad band extending from ~1.3 eV to 1.7 eV electron binding energy. The congested nature of the spectrum is likely due to the presence of multiple isomers of deprotonated indoline, including ring-opened structures. *Published by AIP Publishing.* https://doi.org/10.1063/1.5003978

I. INTRODUCTION

The bicyclic molecule indole is of interest to the fields of biophysics and biochemistry.[1,2] This is in large part due to the fact that indole acts as a chromophore in tryptophan and therefore dominates much of the spectroscopy performed on numerous biological systems with a tryptophan component. The fluorescence of indole is most commonly utilized in spectroscopic studies of biological systems and has been used to probe protein folding/unfolding dynamics, substrate binding, and external quencher accessibility, to name just a few.[2] The importance of indole as a chromophore of tryptophan has symbiotically inspired numerous spectroscopic studies of indole and indole clustered with various partners.[1,3–20] While this scrutiny from the spectroscopic community is partially due to the related biological interest, indole also provides unique spectroscopic challenges due to the complex nature of its vibronic structure.[21,22] Indole is a low symmetry molecule belonging to the C_s point group, and the two lowest level electronic states (^1L_a and ^1L_b) have been shown to be strongly coupled, due in part to both belonging to the same representation.

Despite this interest in indole, there is relatively little known of its thermochemical properties. Similarly, indolide (structure shown below) has not been studied extensively. The gas phase acidity of indole, referring to deprotonation from the N–H site, was studied in 1988 by means of proton transfer equilibria,[23,24] with the result $\Delta_{acid}H^{o}_{298.15K}$ (N–H) = 352 ± 2 kcal/mol, and has not been updated since that time. The electron affinity (EA) of indolyl was reported by Taft and Bordwell[23] to be 2.52 ± 0.20 eV, employing a thermochemical cycle.[25] This result was updated more recently by McKay *et al.*,[26] 2.31 ± 0.15 eV. The EAs of other radical isomers associated with H atom removal from indole have not been studied. However, an upper bound for the bond dissociation energy of the N–H bond in indole was recently obtained by Nix *et al.*[27] by way of photofragment translational energy spectroscopy: $D_0(N–H) \leq 91.2$ kcal/mol.

Structure of Indolide

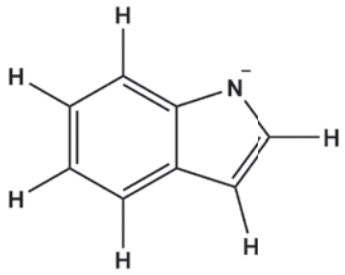

The anion photoelectron spectrum of indolide is presented in this study. These data provide a direct measurement of the electron affinity of the associated neutral, indolyl, with a major increase in precision when compared to the previous measurement. In addition, the vibrations of indolyl that are excited upon electron photodetachment of indolide are measured and assigned with the aid of quantum chemical calculations. Combining the newly measured EA of indolyl with the past measured acidity allows for the determination of the bond dissociation energy with improved accuracy.[25]

II. EXPERIMENTAL

The experimental apparatus has been discussed in detail previously[28,29] and will only be explained briefly here, with special attention as to the generation of the anions of interest. Indole (99% pure) was purchased from Sigma-Aldrich Inc.

[a]Present address: Leybold, Inc., 5700 Mellon Rd., Export, PA 15632, USA.
[b]Author to whom correspondence should be addressed: wcl@jila.colorado.edu

and used without further purification. Crystalline indole has a relatively low vapor pressure and so had to be heated to ~70 °C to obtain adequate indolide production.

The anion of interest is formed in a dual pulsed valve ion source.[29] These valves (Parker Hannifin, General Valve, Series 9) are oriented such that the gas expansions are perpendicular to each other. One of the valves is the primary supersonic expansion (10 psig, ~1% indole or indoline, balance Ar). The other valve, designated as the side valve (35 psig, 1% O_2, 30% H_2, balance Ar), produces about 5% of the total gas load. The side valve has discharge plates placed immediately in front of the valve exit, producing a plasma containing hydroxide. The plasma is subsequently entrained into the supersonic expansion of the primary valve. Upon crossing of the beams, the anions generated in the side valve are allowed to react with the neutral reagents present in the main expansion. Here, the targeted reaction is that of OH^- with indole, which, as will be shown in the subsequent sections, allows for deprotonation at the most acidic site (NH), with the resulting production of indolide anions.[30] This reaction of the hydroxide anion and indole will be shown in Sec. IV to only generate indolide upon reaction with indole. The resultant product and byproducts are then collisionally cooled by the Ar atoms in the main supersonic expansion.

The entrained anions are then extracted into a Time-Of-Flight (TOF) Wiley-McLaren mass spectrometer. The anions are separated by their mass to charge ratio (m/z) and spatially focused at the interaction region of a Velocity Map Imaging (VMI) photoelectron spectrometer. An appropriately timed nanosecond pulse from the photodetachment laser then intersects the anions of a chosen mass. The first stage of the VMI is pulsed to the operating voltage, velocity mapping the photoelectrons onto the plane of a Micro-Channel Plate (MCP) coupled to a phosphor screen and subsequently imaged with a CCD camera. The resulting image gives direct measurement of the two-dimensional velocity distribution. The MEVELER (Maximum Entropy Velocity Legendre Reconstruction) program[31] was used to reconstruct the full three-dimensional velocity distribution of the photoelectrons. This three-dimensional distribution is transformed into the one-dimensional speed distribution and then into the electron Kinetic Energy (eKE) distribution, by means of a Jacobian transform. Finally, the eKE distribution is transformed into the electron Binding Energy (eBE) by simply subtracting the eKE distribution from the photon energy.

The VMI electron energy spectrometer has an energy resolution that depends upon eKE, with the best resolution obtained for the lowest photoelectron kinetic energy. For the experiments reported here, the energy resolution was determined to follow the relation

$$\text{resolution (eKE)} \cong (0.003 + 0.03\ \text{eKE})\ \text{eV}. \quad (1)$$

The constant term is the limiting resolution of the apparatus, in this case 3 meV. The energy scale in the overview spectrum shown in Fig. 1 was calibrated with the known photoelectron spectrum of S^-.[32–34] By employing multiple laser wavelengths, we obtain composite photoelectron spectra spanning several eV, with resolution near the instrumental limit throughout the full range. This procedure is known as Slow Electron Velocity-Map Imaging (SEVI) photoelectron spectroscopy, pioneered by Neumark.[35] The data in Figs. 2 and 3 were obtained at a number of laser wavelengths, chosen so as to take advantage of this higher resolution approach. The photon energies used to obtain these spectra were calibrated with an ATOS λ-meter (LRL–005).

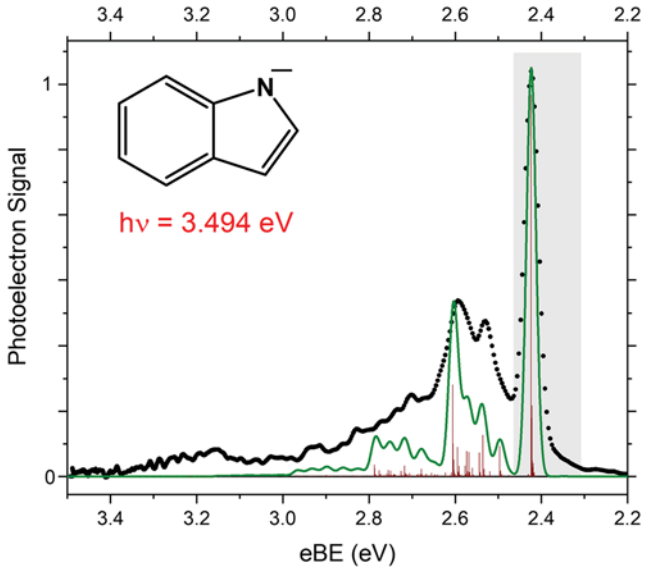

FIG. 1. The photoelectron spectrum of indolide obtained with a photon energy of 3.494 eV. The calculated transitions and their associated intensities are represented by red sticks, while the convolution of these sticks with Gaussian functions whose FWHM is commensurate with the instrument resolution is shown in green. This simulation assumed a temperature of 200 K. The shaded region was obtained in high resolution and is shown in Fig. 2.

All of the spectra shown here are obtained making use of a seeded Nd:YAG pulsed nanosecond laser. The data found in Fig. 1 were obtained utilizing the 3rd harmonic of the Nd:YAG lasing transition (3.494 eV). The spectra shown in Figs. 2 and 3

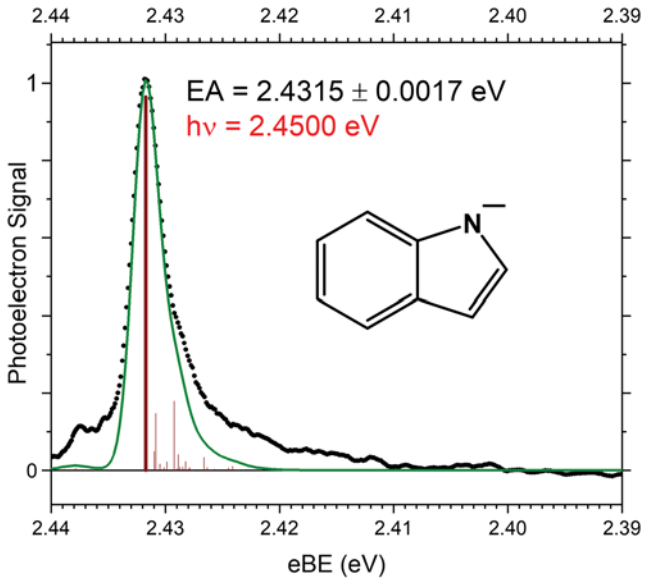

FIG. 2. The Slow Electron Velocity-Map Imaging (SEVI) photoelectron spectrum of the origin transition of indolide acquired with a photon energy of 2.4500 eV. The simulated spectrum is shown in green, with the individual transitions and their respective intensities shown as red sticks. The 0_0^0 transition stick is shown in bold. This simulation assumed a temperature of 200 K.

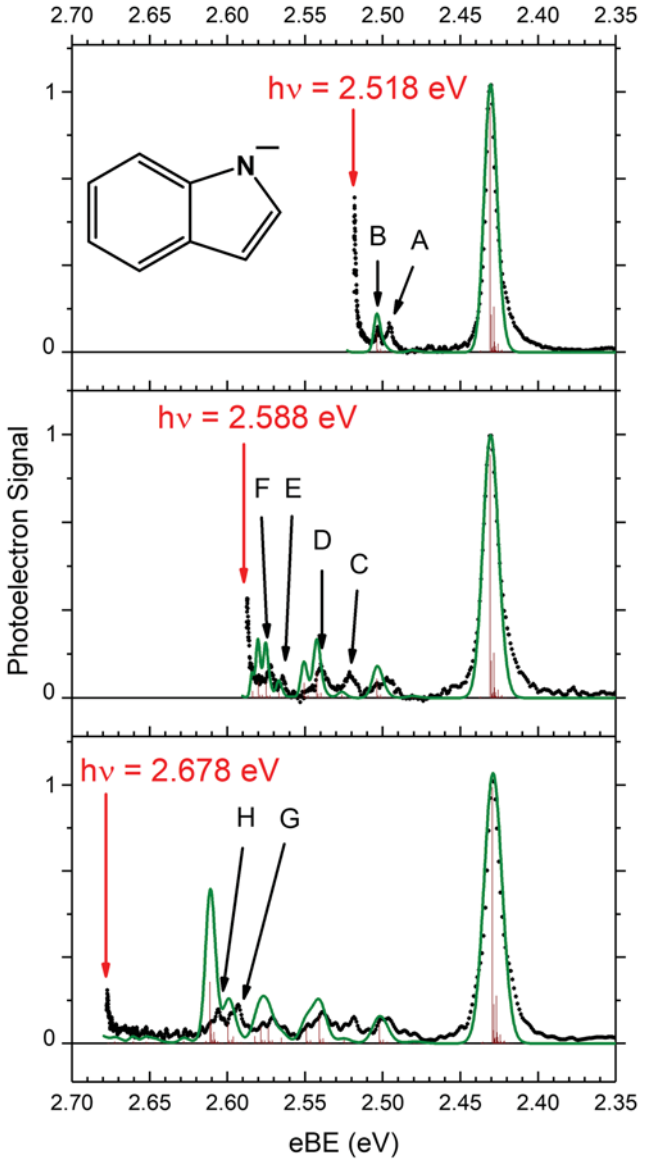

FIG. 3. Photoelectron spectra of indolide obtained with three separate photon energies, 2.518 eV (upper panel), 2.588 eV (middle panel), and 2.678 eV (lower panel). This demonstrates the high resolution of the VMI spectrometer at low electron kinetic energies and takes advantage of this fact. Using this feature, several peaks may be identified and assigned to specific transitions. The sharp rise at near-zero kinetic energy (the highest reported eBE in each panel) is due to the highest resolution of the instrument being within 30 meV of the photon energy. See the main text, supplementary material, and Table II for more information.

were collected utilizing photon energies generated by a visible light optical parametric oscillator (OPO) pumped by the 3rd harmonic of the aforementioned Nd:YAG laser.

Throughout this work, uncertainty in the reported peak positions are functions of the statistical error in finding the peak center, the error in the absolute energy scale, and the number of independent measurements of particular peaks. When reporting the energy associated with a particular transition associated with a peak, the uncertainty in that peak position is combined with the error associated with the offset of the actual transition from the peak center. This aggregated additional uncertainty can be near zero if only a single vibronic transition is the major contributor to the peak shape. If, however, multiple unresolved vibronic transitions contribute significantly to the overall envelope, the uncertainty in location of any individual transition could be as large as the Half-Width-at-Half-Maximum (HWHM) of the peak. Shifts caused by asymmetry in the rotational envelope about each vibrational transition are taken into account using the peak shape analysis of Engelking and co-workers.[36] This rotational correction did not have a significant effect for transitions reported here. In general, the peaks presented in these spectra are comprised of multiple transitions, and the uncertainty associated with these contributions is the dominant component of the reported uncertainties of transition energies.

III. THEORETICAL METHODS

Optimized geometries, electronic structure, and harmonic vibrational normal mode analyses were carried out utilizing the Gaussian 09 program suite.[37] These calculations were performed at the B3LYP/aug-cc-pVTZ level of theory/basis set. This combination has been found to be an effective compromise between accuracy and computational cost.[38] Several excited state calculations were also carried out and made use of Time Dependent Density Functional Theory (TD-DFT) employing the same hybrid functional, B3LYP, and Dunning basis set, aug-cc-pVTZ. All reported EAs are calculated from the Zero-Point Energy (ZPE), the corrected energy difference between the optimized electronic ground neutral state and the optimized electronic ground anionic state.

The optimized geometries and harmonic normal mode analyses were utilized to simulate the photoelectron spectra collected in this experiment and aid in their interpretation. These spectra were simulated assuming that only the Franck–Condon factors (FCFs) influence a given photodetachment transition intensity; i.e., the electronic component of the photodetachment cross section is constant across a given spectrum. Thus, the simulated spectra do not capture behavior such as electron autodetachment. The FCFs were computed via the Sharp–Rosenstock–Chen method, making use of Duschinsky rotations.[39–41] These factors, associated with specific vibrational transitions, along with an assumed 200 K Boltzmann distribution of internal energy in the anions, were computed with the PESCAL program.[42] While these simulations assume full thermal equilibration among the vibrational degrees of freedom of indolide, such is not necessarily the case. These intensities associated with specific transitions are represented as red sticks in Figs. 1–3, where the length of any stick is equal to the calculated intensity of that transition, and it is located at the calculated transition electron binding energy. These transition intensities are converted into simulations of the experimental spectra by convolving each transition with Gaussian functions whose FWHM is commensurate with the instrument resolution, which is a function of eKE, and whose integrated area is equal to that of the calculated transition intensity. The simulations presented are shifted such that the calculated EA matched the observed value. They are also scaled in intensity such that the origin transition of the simulated spectra is in agreement with the peak attributed to the origin transition in the experimental data. This procedure results in the green curves shown in Figs. 1–3.

It is important to underscore several subtleties involved in a Sharp–Rosenstock–Chen FCF analysis of polyatomic photoelectron spectra of species that are as large as indole. This analysis first requires identifying and matching the *molecular motion* of particular vibrations in the anion (in the ground electronic state, for any case shown here) to the molecular motion of vibrations of the neutral in some electronic state. The eigenvectors representing these motions may be found in the supplementary material. Hence, a vibrational normal mode designated as ν_{35} in the anion might be associated, for instance, with ν_{39} in the neutral molecule. While the molecular motion of a particular vibration will be relatively invariant to the level of theory used to compute it, the frequency associated with that eigenvector may shift by ~50 cm^{-1}. Such an energy shift might change what is labeled as ν_{30} at one level of theory to be labeled, for example, ν_{33} in a different level of theory, but the molecular motions will remain largely unchanged and therefore would be matched to the same mode in the anion. This relabeling of normal modes depending on the level of theory utilized will affect both the neutral and the anion. The simulations shown here rely only on the molecular motions to calculate the FCFs; thus while the ordering scheme used here to label the vibrational modes is potentially sensitive to the level of theory one might use, the simulations of the photoelectron spectra are not.

IV. RESULTS

Prior to examining the data, it is useful to hypothesize the likely behaviors one might expect to observe upon photodetachment of deprotonated indole. In the case of indole, it is likely that deprotonation will occur at the N–H site as this must have a much greater acidity than any other site on the molecule. This would result in the formation of an anion which might be expected to have a similar photoelectron spectrum to that of pyrrolide, based on the structural similarity of the molecules. The pyrrolyl radical was shown to have an EA of 2.145 ± 0.010 eV and the photoelectron spectrum of pyrrolide displayed excitation of ring distortion vibrational modes upon photodetachment.[43] Assuming that the EA of indolyl would be close to the EA of pyrrolyl is consistent with our calculation of the EA of indolyl, 2.357 eV. If, however, a ring carbon site is deprotonated, a photoelectron spectrum similar to cyclopentadienide might be expected.[44] Although vibrational structure similar to pyrrolyl was observed upon photodetachment of cyclopentadienide (ring distortion vibrational modes), the EA of cyclopentadienyl radical was measured as 1.808 ± 0.006 eV,[44] a value which is significantly lower than that of the pyrrolyl radical. This analysis implies that if the product of deprotonation from a C–H site on indole was present, we would observe a photoelectron spectrum with an origin ~0.5 eV eBE below the calculated indolyl electron affinity.

In order to examine the above hypotheses, an overview photoelectron spectrum of indolide obtained with a photon energy of 3.494 eV was collected and is shown in Fig. 1. The experimental data are shown as black dots, the calculated Franck–Condon factors appear as red sticks, and the full, shifted theoretical simulation of the photoelectron spectrum of the indolyl ground state is shown as a green curve. The agreement between theory and experiment is qualitatively correct, but the ground state simulation does not appear to account for the weak, broad feature located at approximately 3.2 eV binding energy. As can be seen, the origin of this band is comprised of an intense peak, with a center near 2.4 eV eBE. This result is consistent with the calculation of the EA of indolyl, 2.357 eV (B3LYP/aug-cc-pVTZ), and confirms the formation of the indolide anion. The shaded region was obtained in high resolution (SEVI) and is shown in Fig. 2. No photoelectron signal was observed at lower binding energies, which indicates that indole anions arising from carbon site deprotonation are not present in detectable quantities. Thus, we conclude that the only isomer of deprotonated indole observed is indolide, which does not preclude the other isomers as being thermodynamically possible, simply that they were not observed in this experiment.

The photoelectron spectra presented in this work showed no definitive evidence of the presence of an excited electronic state of indolyl. This result is consistent with the calculated term energy of the first excited electronic state of indolyl being ~1.5 eV and thus would not be accessible with the 3.494 eV photon energy available.

A. Electron affinity of indolyl and photoelectron angular distributions of indolide

In order to obtain the EA of indolyl with a greater degree of accuracy and precision, the SEVI technique was employed. Figure 2 displays the SEVI photoelectron spectrum of the origin peak of the progression shown in Fig. 1 (gray shaded area). Again, the experimental data are shown as black dots, while the green trace and the red sticks represent the shifted simulation and individual calculated harmonic vibrational transitions and their respective intensities. The calculated origin transition, i.e., the transition from the ground electronic and vibrational anionic state to the ground electronic and vibrational state of the neutral radical (0_0^0), has been made bold in the figure. The experimental peak is asymmetric indicating that while the peak primarily arises from the origin transition, other vibrational transitions also contribute. The simulation supports this; while the origin transition dominates the simulated spectrum, there are a number of less significant red-shifted transitions from the origin transition. These additional transitions in the 200 K simulation are the result of sequence-band transitions involving vibrationally excited anions. While observable in the simulations, they do not have a significant effect on the determination of the location of the origin peak, as the fit is limited to an energy range corresponding to roughly the upper 60% of the origin peak, as seen in Fig. 2. This procedure allows for a direct measurement of the position of the intense peak and hence the EA of indolyl, 2.4315 ± 0.0017 eV.

In addition to the electron affinities, photoelectron angular distributions with respect to the laser polarization, characterized by the anisotropy parameter (β), were measured for these photoelectron spectra. Since the electron detached from indolide to form the ground electronic state of indolyl can be described as originating from a nitrogen p-like orbital, it is expected that we should observe an isotropic angular distribution ($\beta \sim 0$) for low kinetic energy photoelectrons which shifts to an anisotropic distribution characterized by

negative values of β at higher kinetic energies.[45,46] This is, in fact, what is observed. In the case of low kinetic energy photoelectrons, such as those found in Figs. 2 and 3, an isotropic angular distribution of all photoelectrons is observed. When utilizing a photon energy of 3.494 eV (Fig. 1), giving rise to photoelectron kinetic energies higher than in the photoelectron spectra found in Figs. 2 and 3, an anisotropic angular distribution of the origin transition was observed, characterized by $\beta \sim -0.25$. This result was anticipated as these photoelectrons possess relatively high kinetic energy (~1 eV) and originate from a p-like molecular orbital.

B. Vibrational analysis of indolyl

Considering the large number of vibrational modes predicted to be activated upon photodetachment of indolide, several spectra were obtained at three different photon energies in an attempt to obtain higher resolution spectra of these vibrational transitions and displayed in Fig. 3. Experimental data are shown in black, while the theoretical modeling is shown as red sticks and green curves. Several observations are immediately apparent. First, in all three spectra there appears to be a large photoelectron signal at near zero eKE (the highest reported eBE in each case). This arises from the high resolution of the instrument at very low eKE (high eBE) combined with many transitions accessible near the photodetachment threshold for all three photon energies employed. Second, the intensity ratios of all peaks relative to the origin transition appear to be qualitatively different from the same ratios in Fig. 1, where the photon energy utilized was higher, 3.494 eV. This is evidence of a photon energy dependence in the photoelectron spectrum of indolide. This is discussed further in Sec. V. In addition to these phenomena, there are several sharp peaks identified in the figure, and a vibrational analysis may be performed as follows.

Assigning any given peak to a specific transition or transitions is a challenging task for a large molecule, such as indolyl, and one must rely heavily upon theoretical simulations. Considering the low symmetry of indolyl (C_s), the ordering convention employed here for the calculated vibrational normal modes is organized first by the allowed symmetries of the vibrational modes (A' or A'') and then by frequency as seen in Table I. Table I also provides each Franck–Condon factor associated with the transition from the ground vibrational state in the anion to one quanta of the appropriate mode (and zero quanta in all other normal modes) in the neutral radical. These transitions are given the shorthand notation of X_0^1, where X refers to the Xth vibrational normal mode which undergoes excitation upon photodetachment of the anion and that all other vibrational normal modes are not excited. The FCFs have been normalized such that the FCF for the origin transition from the anionic ground vibronic state to the neutral ground vibronic state is unity. The energies, molecular motions, and FCFs reported in this table collectively form the basis for the vibrational assignments reported in this work. The harmonic FCFs for the 39 vibrations listed in Table I range from 0.24 to ≪0.01. As the first step in the analysis, we exclude from consideration in our assignment process all neutral vibrational modes with a FCF ≤ 0.01, reducing the number of possible assignments from 39 to 13.

TABLE I. Calculated vibrational analysis of indolyl. Calculated photoelectron harmonic transition energies and their associated FCFs. Note that the notation of X_0^1 implies that all vibrational modes other than vibrational mode X received no quanta of vibrational excitation. The Franck–Condon factors have been normalized such that the vibronic origin transition FCF is unity. Those vibrations which have been positively identified in this work are shown in bold font. While the difference in frequency for many modes may be small (~10 cm^{-1}), the FCF can vary by a factor of up to 1000, and the intensity difference may allow vibrational assignment when calculated energies alone cannot provide a definitive assignment.

$^2\tilde{X}A'$ calculated indolyl harmonic transition energies (cm^{-1})		FCF	$^2\tilde{X}A''$ calculated indolyl harmonic transition energies (cm^{-1})		FCF
1_0^1	3221	<0.01	28_0^1	997	<0.01
2_0^1	3196	<0.01	29_0^1	963	<0.01
3_0^1	3193	<0.01	30_0^1	922	<0.01
4_0^1	3189	<0.01	31_0^1	886	<0.01
5_0^1	3175	<0.01	32_0^1	783	<0.01
6_0^1	3167	<0.01	33_0^1	774	<0.01
7_0^1	1629	<0.01	34_0^1	744	<0.01
8_0^1	1602	0.10	35_0^1	575	<0.01
9_0^1	1495	<0.01	36_0^1	543	<0.01
10_0^1	1466	**0.24**	37_0^1	412	<0.01
11_0^1	1460	**0.07**	38_0^1	241	<0.01
12_0^1	1373	**0.08**	39_0^1	202	<0.01
13_0^1	1346	0.03			
14_0^1	1303	<0.01			
15_0^1	1233	0.03			
16_0^1	1202	0.07			
17_0^1	1169	<0.01			
18_0^1	1162	0.06			
19_0^1	1096	0.02			
20_0^1	1026	<0.01			
21_0^1	966	**0.06**			
22_0^1	899	**0.11**			
23_0^1	854	<0.01			
24_0^1	770	**0.02**			
25_0^1	587	**0.08**			
26_0^1	545	<0.01			
27_0^1	408	<0.01			

Considering the density of vibrational states of both the anion and neutral molecules studied here, computing a given vibrational transition energy and comparing this against the position of the peaks comprising the collected photoelectron spectra cannot result in any firm assignments. Consequently, the computed Franck–Condon factors must be utilized in order to narrow the field of potential vibrational transition assignments to only one or two transitions for a given peak. Even this can only be done if one or two calculated FCFs dominate the predicted intensity of the peak in question. These assignments are further governed by the inherent limitations of relying on the appropriateness of the harmonic oscillator approximation. As such, several assignments made in this work must only be suggested, rather than concretely stated. It is within the limits of these constraints that vibrational transitions are assigned to peaks.

The vibrational analysis begins with the spectrum in the top panel of Fig. 3 with two peaks labeled A and B. The peak centers are located energetically at 521 ± 15 and 577 ± 15 cm^{-1}, respectively, above the origin peak center. The

simulation shown in green overlaid on the data shows one transition with significant intensity in this region, the 25_0^1 transition, with a transition energy calculated as 587 cm^{-1} relative to the origin transition. Hence, peak B may be assigned to the 25_0^1 transition, with a measured transition energy of 577 ± 15 cm^{-1}. Peak A remains unassigned, though it is possible to suggest either 26_0^1 or 27_0^1, based on symmetry and the predicted harmonic frequencies of these vibrational modes. The middle panel of Fig. 3 shows four additional peaks labeled C–F, with peak centers located at 722 ± 15, 870 ± 15, 1071 ± 15, and 1139 ± 15 cm^{-1}, respectively, relative to the origin transition. Several transitions overlap the spectral region containing peak C; however, only one has the proper symmetry and an appreciable FCF, 24_0^1. Hence this is the transition assigned to give rise to peak C with a measured transition energy, relative to the origin transition, of $24_0^1 = 720 \pm 50\ cm^{-1}$. Peak D is predicted to primarily arise from two separate transitions, 22_0^1 and 21_0^1. Considering the proximity of the predicted harmonic vibrational frequencies of these normal modes, the transitions cannot be individually measured. In addition, we cannot verify the presence of both transitions independently, and so either one or both may be contributing to this peak. Hence the transitions are measured to be 22_0^1 and/or $21_0^1 = 870$ ± 80 cm^{-1}, relative to the origin transition. Similarly, peaks E and F, located, respectively, at 1071 ± 15 and 1139 ± 15 cm^{-1} relative to the origin transition peak arise from at least two of the three different transitions with significant predicted FCFs in this region of the photoelectron spectrum, 16_0^1, 18_0^1, and 19_0^1. The bottom panel of Fig. 3 identifies peaks G and H, located at 1314 ± 15 and 1407 ± 15 cm^{-1} higher in binding energy than the origin peak. Peak G arises primarily from the 12_0^1 transition, and thus a transition energy may be determined, 1310 ± 35 cm^{-1} above the origin. Peak H is predicted to be dominated by two separate transitions with calculated harmonic frequencies inseparably close to each other, 11_0^1 and 10_0^1. Similar to the situation for peak D, there is no experimental way to prove the contribution of either transition to the peak H line shape, though the 11_0^1 transition is theoretically predicted to have a FCF ~3.4 times larger than the 10_0^1 transition. Thus the transitions associated with Peak H are assigned as 11_0^1 and/or 10_0^1 = 1400 ± 70 cm^{-1}, relative to the origin. These results are summarized in Table II.

TABLE II. Summary of experimental vibrational assignments. Vibrational analysis of the indolide photoelectron spectrum found in Fig. 3. Vibrational mode assignments for Peaks A, E, and F could not be made to the level of confidence necessary to report in this table. Several suggested assignments are presented in the main text for these unassigned peaks.

Peak	Position relative to 0_0^0 (cm^{-1})	Assignment (cm^{-1})
A	521 ± 15	
B	577 ± 15	$25_0^1 = 580 \pm 25$
C	722 ± 15	$24_0^1 = 720 \pm 50$
D	870 ± 15	22_0^1 and/or $21_0^1 = 870 \pm 80$
E	1071 ± 15	
F	1139 ± 15	
G	1314 ± 15	$12_0^1 = 1310 \pm 35$
H	1407 ± 15	11_0^1 and/or $10_0^1 = 1400 \pm 70$

All of the above assigned vibrational transitions are associated with vibrational normal modes which are of A' symmetry and can be described as ring distortion motions. The eigenvectors associated with these normal modes may be found in the supplementary material.

C. Deprotonated indoline

In addition to the photoelectron spectrum of indolide, an attempt was made to also collect the photoelectron spectrum of deprotonated indoline. The results of this measurement may be found in the supplementary material for the primary purpose of providing a record. The actual spectrum is not included in the main text because the photoelectron spectrum of deprotonated indoline, while predicted to look much like that of indolide, was broad and featureless, but with a photodetachment onset observed near the calculated EA of the indolinyl radical, 1.291 eV. The observed congestion is likely due to multiple isomers of deprotonated indoline generated in the ion source, including ring opened structures.

V. DISCUSSION

The EA of indolyl was measured to be 2.4315 ± 0.0017 eV. This value may be compared to previous studies of indolyl in the literature. The EA of the indolyl radical has been measured twice previously.[23,26] In the case of Taft and Bordwell,[23] this is accomplished by means of applying a thermochemical cycle to their proton transfer equilibria data, and thus the EA was determined to be 2.52 ± 0.20 eV. This value was later updated in 2010 by McKay *et al.*,[26] utilizing anion photoelectron spectroscopy to find an EA of 2.31 ± 0.15 eV. This present work is in agreement with these two past studies and greatly improves the accuracy of the measurement of the EA of the indolyl radical.

Several structural analogs of indolyl may also be examined and compared to the measured EA of indolyl: pyrrolyl, phenyl, cyclopentadienyl, and cyclopentyl radical.[43,47,48] One may think of pyrrolide as an analog of indolide, while phenide or cyclopentadienide may represent indole deprotonated at a carbon site. The pyrrolyl radical was shown to have an EA of 2.145 ± 0.010 eV, while the EAs of phenyl and cyclopentadienyl are 1.096 ± 0.006 eV and 1.808 ± 0.006 eV, respectively.[43,47,48] Both analogs of carbon site deprotonation display a lower EA than pyrrolyl radical, wherein the excess charge on the anion is concentrated about the nitrogen atom. This is consistent with the EA of indolide, 2.4315 ± 0.0017 eV, and demonstrates that the EA of pyrrolyl radical is not greatly perturbed by the addition of a fused aromatic ring to the structure, resulting in indolyl. This is expected; the pyrrolyl ring is aromatic and the addition of another aromatic ring, which is neither strongly electron donating nor withdrawing, to the conjugated π system will not significantly disrupt the qualitative aspects of the aromatic electronic structure.

The eKE dependence of the photoelectron angular distributions of indolide are now considered. The data indicate that the photodetached electrons from indolide originate in a π system, based on the negative β parameter.[45,46] This interpretation may be somewhat surprising, as in this case

the aromaticity arises from both π and σ bonds. However, this observation is consistent with our electronic structure calculations, which show that the HOMO of indolide is a classic π system ring. Additionally, this behavior has been observed for many other aromatic anions when photoelectron angular distributions were obtained.[47,49]

Upon electron photodetachment from indolide, several vibrational modes are excited; the eigenvectors associated with these vibrational modes may be found in the supplementary material. All of the modes that are activated upon photodetachment share two characteristics. First, they are all of A' symmetry and so preserve the only plane of symmetry of the molecular point group, C_s, which is also the plane of the molecule itself. Second, all of the observed vibrational modes describe molecular motion that can be characterized as ring distortions. This behavior has been observed in aromatic anion photoelectron spectroscopy previously.[43,44,47,49] Both of these observations are intuitively understandable. Indolide will have the excess charge density primarily localized about the nitrogen group. This increased charge density will cause the bonds along the fused aromatic ring structure to lengthen from an idealized pyrrole-like structure, while preserving the C_s symmetry. Upon photodetachment, the new equilibrium geometry will be closer to that of pyrrole, causing vibrational motion to be activated which incorporates displacements along the bonds which make up the fused aromatic ring, resulting in both vibrations which do not break the symmetry of the molecule and which one might describe as ring distortion motion.

The intensities of peaks seen in the photoelectron spectrum of indolide change as a function of photon energy. This can be observed by a comparison of the 3.494 eV photoelectron spectrum displayed in Fig. 1 with the photoelectron spectra displayed in Fig. 3, obtained with several photon energies ∼1 eV lower than 3.494 eV. For example, in the bottom panel of Fig. 3 one may note that the ratio of the intensity of peak H to the origin transition peak is different from the same ratio in Fig. 1. This ratio in Fig. 3 is far lower than what is found in Fig. 1. This variability in peak intensity ratios cannot be explained by threshold effects. This variation must be due to electron autodetachment in competition with direct photodetachment, a behavior that has been observed in other aromatic systems.[47,49–51] This conclusion is borne out in excited state quantum chemical calculations (TD-DFT) of the indolide anion which predict 9 optically accessible electronic states with term energies ranging from 2.5 to 3.6 eV above the ground vibronic state energy. Due to the density of the available states and the inherent complexity of autodetachment, it is beyond the scope of this work to further investigate this phenomenon theoretically.

The thermodynamic implications of the improved measurement of the EA of indolyl are now considered. We utilize a thermochemical cycle[25] that combines the EA of indolyl with an accurate determination of an upper bound for the indole N–H bond dissociation energy by Nix *et al.*,[27] $D_0(\text{N–H}) \leq 91.2$ kcal/mol, to obtain a lower bound for the gas phase acidity of indole. This cycle yields an upper bound to the gas phase acidity as $\Delta_{acid}H^o_{0K}(\text{N–H})_{indole} \leq 348.7$ kcal/mol. We convert this 0 K value to standard temperature (298.15 K) by means of the calculated heat capacities of the species involved in the acid reaction: $\text{indole}_{(g)} \rightarrow \text{H}^+_{(g)} + \text{indolide}_{(g)}$,

$$\Delta_{acid}H^o_{298.15K}\,(\text{indole}) = \Delta_{acid}H^o_{0K}\,(\text{indole}) + \int_{0K}^{298.15K}\left[C_p\,(\text{indolide}) + C_p\,(\text{H}^+) - C_p\,(\text{indole})\right]\text{dT}. \quad (2)$$

This procedure yields $\Delta_{acid}H^o_{298.15K}(\text{N–H})_{indole} \leq 350.2$ kcal/mol. Comparing this upper bound with the value reported by Meot–Ner *et al.*[24] ($\Delta_{acid}H^o_{298.15K}(\text{N–H})_{indole} = 352 \pm 2$ kcal/mol), we note that it is just barely within the error bars reported by Meot–Ner *et al.*[24] Considering the accuracy of our EA measurement (±0.04 kcal/mol), combined with the proximity of the upper limit to the true bond strength that is typical of the method employed by Ashfold and coworkers[27] (∼100 cm^{-1} or ∼0.3 kcal/mol), we believe that the value reported by Meot-Ner *et al.* for $\Delta_{acid}H^o_{298.15K}(\text{N–H})_{indole}$ likely overestimates the actual acidity of indole. Although the difference is not substantial, the upper bound reported in this work provides a more reliable determination of $\Delta_{acid}H^o_{298.15K}(\text{N–H})_{indole}$. Given the usual accuracy and precision of high resolution photofragment spectroscopy employed by Nix *et al.*,[27] we expect that our measurement of the gas phase acidity (≤348.7 kcal/mol at 0 K) lies no more than a few hundred wavenumbers below the reported upper bound, i.e., the gas phase acidity of indole is very likely to be $\Delta_{acid}H^o_{0K}(\text{N–H})_{indole} \approx 348.7 \pm 0.5$ kcal/mol.

VI. CONCLUSION

The anion photoelectron spectra of deprotonated indole and indoline have been collected utilizing several photon energies in order to take advantage of the high resolution associated with slow electrons in this apparatus. The SEVI photoelectron spectrum of indolide shows the EA of indolyl to be 2.4315 ± 0.0017 eV. Indolide photodetachment activates numerous ring distortion vibrations of A' symmetry. Previous work studying the dissociation energy of H-indolyl[27] allows for a new independent measure of $\Delta_{acid}H^o_{0K}(\text{N–H})_{indole} \leq 348.7$ kcal/mol, which improves the previous measurement of the gas phase acidity reported by Meot-Ner *et al.*[24] The photoelectron spectrum of deprotonated indoline exhibited far more spectral congestion than was anticipated, apparently a result of the presence of multiple isomers of deprotonated indoline, although specific identification was not possible. The relative intensities of vibrations excited in the photoelectron spectrum of indolide displayed a strong photon energy dependence, the result of electron autodetachment.

SUPPLEMENTARY MATERIAL

See supplementary material for additional photoelectron spectra of indolide that were deemed peripheral to the focus of this work, as well as the photoelectron spectrum of deprotonated indoline, and calculated eigenvectors representing the harmonic normal mode motion of indolyl.

ACKNOWLEDGMENTS

The authors gratefully acknowledge support from NSF Grant No. PHY1734006. The authors also wish to

acknowledge insightful conversations concerning the intricacies of indolide with Dr. Julia H. Lehman of the University of Leeds.

[1]E. H. Strickland, J. Horwitz, and C. Billups, Biochemistry **9**, 4914 (1970).
[2]J. T. Vivian and P. R. Callis, Biophys. J. **80**, 2093 (2001).
[3]J. R. Carney and T. S. Zwier, J. Phys. Chem. A **103**, 9943 (1999).
[4]J. R. Carney, F. C. Hagemeister, and T. S. Zwier, J. Chem. Phys. **108**, 3379 (1998).
[5]G. A. Bickel, D. R. Demmer, E. A. Outhouse, and S. C. Wallace, J. Chem. Phys. **91**, 6013 (1989).
[6]J. Hager, M. Ivanco, M. A. Smith, and S. C. Wallace, Chem. Phys. Lett. **113**, 503 (1985).
[7]J. Hager and S. C. Wallace, J. Phys. Chem. **87**, 2121 (1983).
[8]S. Arnold and M. Sulkes, J. Phys. Chem. **96**, 4768 (1992).
[9]C. K. Teh, J. Sipior, and M. Sulkes, J. Phys. Chem. **93**, 5393 (1989).
[10]G. Berden, W. L. Meerts, and E. Jalviste, J. Chem. Phys. **103**, 9596 (1995).
[11]M. J. Tubergen and D. H. Levy, J. Phys. Chem. **95**, 2175 (1991).
[12]C. Unterberg, A. Jansen, and M. Gerhards, J. Chem. Phys. **113**, 7945 (2000).
[13]W. Caminati and S. Di Bernardo, J. Mol. Struct. **240**, 253 (1990).
[14]R. D. Suenram, F. J. Lovas, and G. T. Fraser, J. Mol. Spectrosc. **127**, 472 (1988).
[15]Y. Nibu, H. Abe, N. Mikami, and M. Ito, J. Phys. Chem. **87**, 3898 (1983).
[16]B. J. Fender, D. M. Sammeth, and P. R. Callis, Chem. Phys. Lett. **239**, 31 (1995).
[17]W. B. Collier, J. Chem. Phys. **88**, 7295 (1988).
[18]S. Albert, K. K. Albert, P. Lerch, and M. Quack, Faraday Discuss. **150**, 71 (2011).
[19]J. M. Hollas, Spectrochim. Acta **19**, 753 (1963).
[20]R. Bersohn, U. Even, and J. Jortner, J. Chem. Phys. **80**, 1050 (1984).
[21]L. Serrano-Andrés and B. O. Roos, J. Am. Chem. Soc. **118**, 185 (1996).
[22]J. Kupper, D. W. Pratt, W. Leo Meerts, C. Brand, J. Tatchen, and M. Schmitt, Phys. Chem. Chem. Phys. **12**, 4980 (2010).
[23]R. W. Taft and F. G. Bordwell, Acc. Chem. Res. **21**, 463 (1988).
[24]M. Meot-Ner, J. F. Liebman, and S. A. Kafafi, J. Am. Chem. Soc. **110**, 5937 (1988).
[25]K. M. Ervin and V. F. DeTuri, J. Phys. Chem. A **106**, 9947 (2002).
[26]A. R. McKay, M. E. Sanz, C. R. S. Mooney, R. S. Minns, E. M. Gill, and H. H. Fielding, Rev. Sci. Instrum. **81**, 123101 (2010).
[27]M. G. D. Nix, A. L. Devine, B. Cronin, and M. N. R. Ashfold, Phys. Chem. Chem. Phys. **8**, 2610 (2006).
[28]L. Sheps, E. M. Miller, and W. C. Lineberger, J. Chem. Phys. **131**, 064304 (2009).
[29]Y.-J. Lu, J. H. Lehman, and W. C. Lineberger, J. Chem. Phys. **142**, 044201 (2015).
[30]B. Ruscic, A. F. Wagner, L. B. Harding, R. L. Asher, D. Feller, D. A. Dixon, K. A. Peterson, Y. Song, X. Qian, C.-Y. Ng, J. Liu, W. Chen, and D. W. Schwenke, J. Phys. Chem. A **106**, 2727 (2002).
[31]B. Dick, Phys. Chem. Chem. Phys. **16**, 570 (2014).
[32]H. Hotop and W. C. Lineberger, J. Phys. Chem. Ref. Data **14**, 731 (1985).
[33]T. Andersen, H. K. Haugen, and H. Hotop, J. Phys. Chem. Ref. Data **28**, 1511 (1999).
[34]C. Blondel, W. Chaibi, C. Delsart, C. Drag, F. Goldfarb, and S. Kröger, Eur. Phys. J. D **33**, 335 (2005).
[35]D. M. Neumark, J. Phys. Chem. A **112**, 13287 (2008).
[36]M. J. Travers, D. C. Cowles, E. P. Clifford, G. B. Ellison, and P. C. Engelking, J. Chem. Phys. **111**, 5349 (1999).
[37]M. J. Frisch, G. W. Trucks, H. B. Schlegel, G. E. Scuseria, M. A. Robb, J. R. Cheeseman, G. Scalmani, V. Barone, B. Mennucci, G. A. Petersson, H. Nakatsuji, M. Caricato, X. Li, H. P. Hratchian, A. F. Izmaylov, J. Bloino, G. Zheng, J. L. Sonnenberg, M. Hada, M. Ehara, K. Toyota, R. Fukuda, J. Hasegawa, M. Ishida, T. Nakajima, Y. Honda, O. Kitao, H. Nakai, T. Vreven, J. A. Montgomery, J. E. Peralta, F. Ogliaro, M. Bearpark, J. J. Heyd, E. Brothers, K. N. Kudin, V. N. Staroverov, R. Kobayashi, J. Normand, K. Raghavachari, A. Rendell, J. C. Burant, S. S. Iyengar, J. Tomasi, M. Cossi, N. Rega, J. M. Millam, M. Klene, J. E. Knox, J. B. Cross, V. Bakken, C. Adamo, J. Jaramillo, R. Gomperts, R. E. Stratmann, O. Yazyev, A. J. Austin, R. Cammi, C. Pomelli, J. W. Ochterski, R. L. Martin, K. Morokuma, V. G. Zakrzewski, G. A. Voth, P. Salvador, J. J. Dannenberg, S. Dapprich, A. D. Daniels, Farkas, J. B. Foresman, J. V. Ortiz, J. Cioslowski, and D. J. Fox, GAUSSIAN 09, Revision B.01, Gaussian, Inc., 2009, see http://gaussian.com/.
[38]A. D. Becke, J. Chem. Phys. **98**, 5648 (1993).
[39]T. E. Sharp and H. M. Rosenstock, J. Chem. Phys. **41**, 3453 (1964).
[40]E. B. Wilson, Jr., Phys. Rev. **45**, 706 (1934).
[41]P. Chen, *Unimolecular and Bimolecular Reactions Dynamics* (John Wiley & Sons, Chichester, 1994), p. 371.
[42]K. M. Ervin, PESCAL, Fortran Program for Franck-Condon Analysis of Molecular Photoelectron Spectra, see http://wolfweb.unr.edu/~ervin/pes/.
[43]A. J. Gianola, T. Ichino, R. L. Hoenigman, S. Kato, V. M. Bierbaum, and W. C. Lineberger, J. Phys. Chem. A **108**, 10326 (2004).
[44]T. Ichino, S. W. Wren, K. M. Vogelhuber, A. J. Gianola, W. C. Lineberger, and J. F. Stanton, J. Chem. Phys. **129**, 084310 (2008).
[45]J. Cooper and R. N. Zare, J. Chem. Phys. **48**, 942 (1968).
[46]A. Sanov, Annu. Rev. Phys. Chem. **65**, 341 (2014).
[47]R. F. Gunion, M. K. Gilles, M. L. Polak, and W. C. Lineberger, Int. J. Mass Spectrom. Ion Processes **117**, 601 (1992).
[48]C. H. DePuy, S. Gronert, S. E. Barlow, V. M. Bierbaum, and R. Damrauer, J. Am. Chem. Soc. **111**, 1968 (1989).
[49]D. J. Nelson, W. K. Gichuhi, E. M. Miller, J. H. Lehman, and W. C. Lineberger, J. Chem. Phys. **146**, 074302 (2017).
[50]C. S. Anstöter, C. R. Dean, and J. R. R. Verlet, J. Phys. Chem. Lett. **8**, 2268 (2017).
[51]L.-S. Wang, J. Chem. Phys. **143**, 040901 (2015).